

Polarized Radiation Signals from Highly Magnetized Neutron Star Surfaces

Kun Hu¹, Matthew G. Baring¹, Joseph A. Barchas² and George Younes³

¹ Department of Physics and Astronomy - MS 108, Rice University,
6100 Main St., Houston, TX 77251-1892, USA

² Natural Sciences, Southwest Campus, Houston Community College,
5601 W. Loop S., Houston, Texas 77081, USA

³ Astrophysics Science Division, NASA Goddard Space Flight Center,
Greenbelt, MD 20771, USA

Abstract. The surfaces of neutron stars are likely sources of strongly polarized soft X rays due to the presence of strong magnetic fields. Scattering transport in the surface layers is critical to the determination of the emergent anisotropy of light intensity, and is strongly influenced by the complicated interplay between linear and circular polarization information. We have developed a magnetic Thomson scattering simulation to model the outer layers of fully-ionized atmospheres in such compact objects. Here we summarize emergent intensities and polarizations from extended atmospheric simulations, spanning considerable ranges of magnetic colatitudes. General relativistic propagation of light from the surface to infinity is fully included. The net polarization degrees are moderate and not very small when summing over a variety of field directions. These results provide an important foundation for observations of magnetars to be acquired by NASA's new IXPE X-ray polarimeter and future X-ray polarimetry missions.

Keywords. magnetic fields, stars: neutron, pulsars: general

1. Introduction

The soft X-ray thermal emission from the surfaces of neutron stars provides paths to understanding their surfaces and interiors. Pulse profiles of isolated neutron stars have been used to constrain the geometric parameters for different types of neutron stars; e.g., see Gotthelf et al. (2010) for an example of the central compact object PSR J0821-4300 and Younes et al. (2020) for the magnetar 1RXS J170849.0-400910. Accurate interpretations of the observed surface emission require a sophisticated understanding of the surface layer of neutron stars. Fully or partially-ionized atmospheres of neutron stars have been extensively studied by many groups (Shibanov et al. 1992, Pavlov et al. 1994, Potekhin et al. 2004). Ionized atmosphere models in the magnetar domain were constructed by Özel (2001) and Ho & Lai (2001) and several later papers. In addition, thermal emission from condensed neutron star surfaces at relatively low temperatures has been studied by Medin & Lai (2006) and Medin & Lai (2007). A common feature of these and a number of other previous studies on neutron star atmospheres is that they solve the radiative transfer equations in terms of two orthogonal polarization modes.

In this paper, we present sample results from our Monte Carlo simulation *MAGTH-OMSCATT* that treats the radiation transport in scattering-dominated neutron star atmospheres. It can be applied to neutron stars with a wide range of magnetizations, spanning CCO pulsars to magnetars. Our results provide a more refined determination of the intensity and polarization signatures from the neutron star atmospheres at differ-

ent surface locales, helping to improve the interpretation of neutron star pulse profiles and future X-ray polarization observations. See Hu et al. (2022) for a full exposition.

2. Monte Carlo Simulation of Radiative Transfer

The *MAGTHOMSCATT* simulation treats the radiative transfer of polarized soft X-ray photons in the magnetic Thomson domain (e.g., Herold 1979). It is suitably applied to the outer atmospheres of neutron stars where scatterings generally dominate the opacity. The simulation code adopts a complex electric field vector approach, which is numerically efficient when tracking photon polarizations during atmospheric radiative transfer and also for general relativistic propagation through the magnetosphere. The electric field vectors encapsulate full polarization information and capture the profound interplay between linear and circular polarizations during scatterings. Stokes parameters are generated at the output interface when collecting photons at infinity.

In the simulation, photons are injected at the base of the atmosphere with specified polarization and anisotropy, i.e. Stokes parameters. Our adopted injection captures the precise polarization and anisotropy information from the high opacity solutions of radiation transfer due to Thomson scattering deep inside the atmosphere. Accordingly, thick atmospheres can be simulated efficiently with slabs of moderate opacities, $\tau_{\text{eff}} = 5 - 50$. The design and validation of the *MAGTHOMSCATT* code is detailed in Barchas, Hu & Baring (2021) and Hu et al. (2022).

3. Polarization from Localized and Extended Atmospheres

It is insightful to explore how the emergent anisotropy and polarization depend on the photon frequency for localized atmospheric slabs. Fig. 1 displays the intensity and polarization information for monochromatic radiation emergent from the top of slabs, in the local inertial frame at the stellar surface. In each panel, the magnetic field is tilted at an angle $\theta_B = 15^\circ$ to the local zenith. This choice is germane to neutron star emission models where radiation from hot polar caps dominates the observed flux. The photon

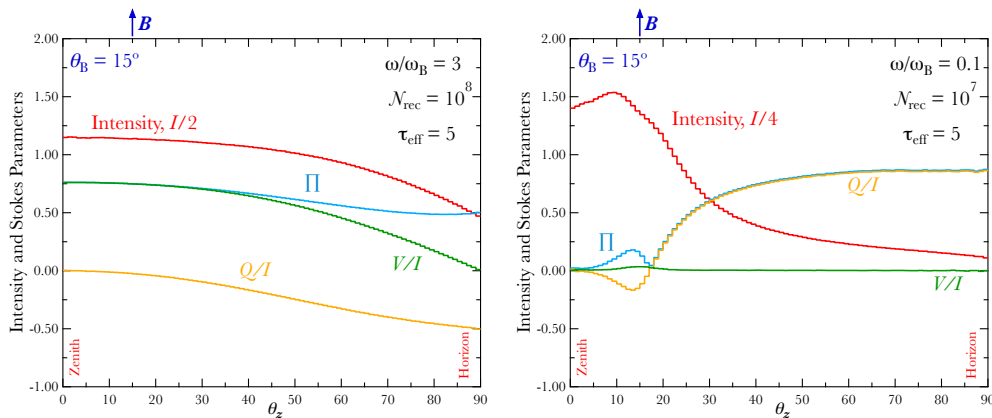


Figure 1. Angular distributions of the intensity I , Stokes Q/I , Stokes V/I and total polarization degree Π , as functions of zenith angle θ_z , for an atmosphere with \mathbf{B} inclined at $\theta_B = 15^\circ$ to the zenith. They are for monochromatic photons with $\omega/\omega_B = 3$ (left) and $\omega/\omega_B = 0.1$ (right). The effective optical depth for unpolarized photons is $\tau_{\text{eff}} = 5$, (see Hu et al. 2022 for the definition) and the total number of recorded photons $\mathcal{N}_{\text{rec}} = 10^7, 10^8$, as indicated. The intensities are scaled by factors of $1/2$ (left) and $1/4$ (right) to aid clarity of their depiction.

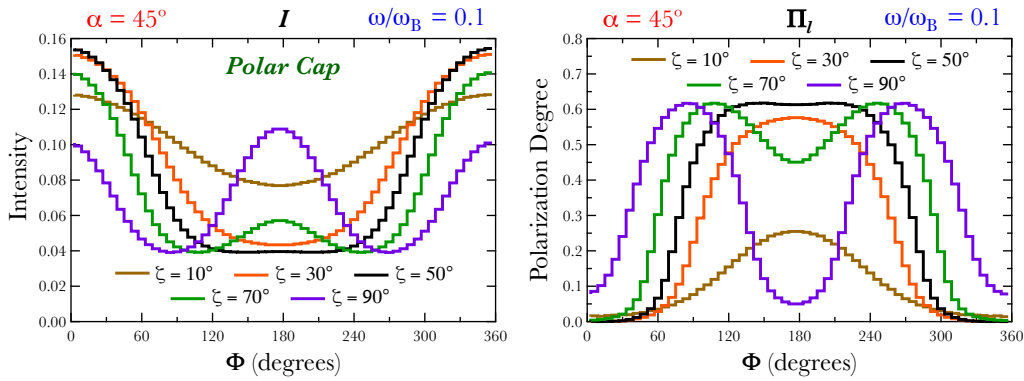


Figure 2. Pulse profiles of intensity I (left) and linear polarization degree Π_l (right) for a rotating neutron star with inclination angle $\alpha = 45^\circ$ between the magnetic moment and spin axes. The emission zone is a uniformly emitting polar cap of $\theta_{\text{cap}} = 30^\circ$ extent in magnetic colatitude. The profiles are plotted as functions of the rotational phase Φ for selected viewing angles $\zeta = 10^\circ, 30^\circ, \dots, 90^\circ$ to the spin axis. The photon frequency is fixed at $\omega = 0.1\omega_B$.

frequencies ω are scaled by the cyclotron frequency $\omega_B = eB/m_e c$. The intensity I , Stokes parameters Q , V and total polarization degree $\Pi = \sqrt{Q^2 + U^2 + V^2}/I$ are integrated over the azimuthal angles about the local zenith and are plotted as functions of the zenith angle θ_z of the emergent radiation. The left panel of Fig. 1 presents results at $\omega/\omega_B = 3$. This approximates the “low-field” $\omega \gg \omega_B$ domain, in which case the field has limited impact on the scattering process and associated diffusion. The intensity distribution manifests a moderate anisotropy. Linear \perp mode polarization prevails ($Q/I < 0$) when the zenith angle is not too small. The Stokes V is strongest along the zenith direction, reflecting the gyration motion induced in “radiating” electrons during scatterings. The left panel of Fig. 1 presents results at $\omega/\omega_B = 0.1$, i.e., the strong field domain ($\omega \ll \omega_B$) where magnetic field strongly affects the scattering process. In this case, the intensity is strongly beamed at small zenith angles close to the magnetic field direction, and \parallel mode photons dominate ($Q/I > 0$) the emergent radiation, a consequence of the character of the cross section: see Barchas, Hu & Baring (2021).

Next, we illustrate the intensity and polarization signatures from extended atmospheric regions. This is achieved by sampling the emission locales for each photon uniformly across the pertinent surface region, mimicking isothermal conditions. General relativistic light bending and the parallel transport of the polarization vectors to infinity are now treated, assuming $M = 1.44M_\odot$ and $R_{\text{NS}} = 10^6$ cm for the star. In Fig. 2, the simulated intensity I and linear polarization degree $\Pi_l = \sqrt{Q^2 + U^2}/I$ are plotted as functions of rotational phase Φ for different viewing directions ζ and a fixed inclination angle $\alpha = 45^\circ$; both angles are measured relative to the stellar rotation axis. The emission regions are chosen to be two antipodal polar caps with half-opening angles equal to 30° , and the photon frequency ratio is set to $\omega/\omega_B = 0.1$. The intensity profiles demonstrate a strong rotational modulation with a pulse fraction $\lesssim 50\%$. The maximum linear polarization degree Π_l is around 60%. This Π_l is very high because the depolarization induced by sampling photons from emission locales with different field directions is reduced when restricting locales to polar caps. This high polarization degree is of interest to NASA’s recently launched IXPE, and also future X-ray polarimeters.

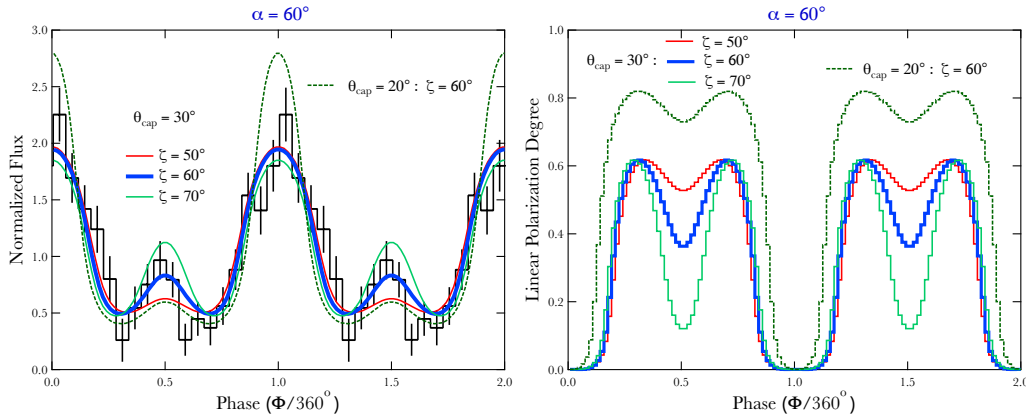


Figure 3. *Left:* Simulated pulse profiles for intensity I for two antipodal polar caps extending from the respective magnetic poles to colatitudes of $\theta_{\text{cap}} = 30^\circ$. The histogram represents the data in Fig. 3 (right) of Younes et al. (2020) for the flare contribution to persistent emission of 1RXS J1708-40. The theoretical models center on the pulse profile (heavyweight, blue) for $\alpha = 60^\circ = \zeta$, which was the system configuration that gave the best statistical fit to the observations. The other two solid curves are for models in the parametric neighborhood with ζ values as labeled. The dotted green curve is for a smaller polar cap with $\theta_{\text{cap}} = 20^\circ$. *Right:* The linear polarization Π_l pulsation traces corresponding to the intensity curves on the left.

4. Observational Diagnostic Potential

Given the strong sensitivity of emission to the stellar geometric angles α , ζ , and the surface distribution of emission locales, we can compare predictions from *MAGTHOM-SCATT* with observed intensity pulse profiles. We performed an exercise of constraining the geometric parameters of the magnetar 1RXS J1708-40. Intensity pulse profiles for models with different geometric parameters are plotted in the left panel of Fig. 3, with the best-fit one displayed as blue, indicating a preferred viewing angle $\zeta \sim 60^\circ$ to the spin axis. The choice of $\omega = 0.1\omega_B$ was made for expediency, generating good statistics with reasonable run times. Since the dominant contribution to the signal comes from $\sim 15^\circ - 30^\circ$ colatitudes, the typical emergent photon angles sampled relative to the local \mathbf{B} direction are large enough that the cross section is somewhat insensitive to the choice of ω , obviating the need to treat slow $\omega \sim 10^{-4}\omega_B$ runs. The right panel presents the pulse profiles of linear polarization degrees for selected models. Refined probes of the geometry parameters can be acquired once phase-resolved polarization observations are available: for brighter magnetars, IXPE is likely to deliver such during the coming year.

References

- Barchas, J. A., Hu, K. & Baring, M. G. 2021, *MNRAS*, 500, 5369.
 Gotthelf, E. V., Perna, R., & Halpern, J. P. 2010, *ApJ*, 724, 1316.
 Herold, H. 1979, *Phys. Rev. D*, 19, 2868.
 Ho, W. C. G., & Lai, D. 2001, *MNRAS*, 327, 1081.
 Hu, K., Baring, M. G., Barchas, J. A. & Younes, G. 2022, *ApJ*, 928, 82.
 Medin, Z., Lai, D. 2006, *Phys. Rev. A*, 74, 062508.
 Medin, Z., Lai, D. 2007, *MNRAS*, 382, 1833.
 Özel, F. 2001, *ApJ*, 563, 276.
 Pavlov, G. G., Shibano, Yu. A., Ventura, J., et al. 1994, *A&A*, 289, 837.
 Potekhin, A. Y., Lai, D., Chabrier, G., et al. 2004, *ApJ*, 612, 1034
 Shibano, Yu. A., Zavlin, V. E., Pavlov, G. G., et al. 1992, *A&A*, 266, 313.
 Younes, G., Baring, M. G., Kouveliotou, C., et al. 2020, *ApJL*, 889, L27.